

The Fragility of Thermoelectric Power Factor in Cross-Plane Superlattices in the Presence of Nonidealities: A Quantum Transport Simulation Approach

M. THESBERG,^{1,3,4} M. POURFATH,¹ N. NEOPHYTOU,² and H. KOSINA¹

1.—Institute for Microelectronics, TU Wien, Gusshausstrasse 27-29/E360, 1040 Vienna, Austria.
2.—University of Warwick, Coventry CV4 7AL, UK. 3.—e-mail: mischa.thesberg@gmail.com.
4.—e-mail: thesberg@iue.tuwien.ac.at

Energy filtering has been put forth as a promising method for achieving large thermoelectric power factors in thermoelectric materials through Seebeck coefficient improvement. Materials with embedded potential barriers, such as cross-plane superlattices, provide energy filtering, in addition to low thermal conductivity, and could potentially achieve high figure of merit. Although there exist many theoretical works demonstrating Seebeck coefficient and power factor gains in idealized structures, experimental support has been scant. In most cases, the electrical conductivity is drastically reduced due to the presence of barriers. In this work, using quantum-mechanical simulations based on the nonequilibrium Green's function method, we show that, although power factor improvements can theoretically be observed in optimized superlattices (as pointed out in previous studies), different types of deviations from the ideal potential profiles of the barriers degrade the performance, some nonidealities being so significant as to negate all power factor gains. Specifically, the effect of tunneling due to thin barriers could be especially detrimental to the Seebeck coefficient and power factor. Our results could partially explain why significant power factor improvements in superlattices and other energy-filtering nanostructures mainly fail to be realized, despite theoretical predictions.

Key words: Thermoelectric, superlattices, quantum transport, thermoelectric power factor, Seebeck coefficient, energy filtering

INTRODUCTION

The thermoelectric (TE) performance of materials is determined by the figure of merit $ZT = \sigma S^2 / \kappa$, where σ denotes the electrical conductivity, S the Seebeck coefficient, and κ the thermal conductivity. Large improvements in ZT have recently been reported in nanoscale materials due to drastic reduction in κ .^{1,2} On the other hand, efforts to improve the power factor (σS^2) have met with less success, and overall ZT still remains low. Energy filtering in nanocomposite materials with embedded potential barriers (of height V_B) is a promising way to improve σS^2 via improve-

ments of the Seebeck coefficient.^{2–18} Cross-plane superlattices were some of the first structures considered to utilize energy filtering.^{3,6,7,9} In these structures, although the theoretical expectation of power factor gains is high ($\sim 40\%$),^{5,10,11,15} accompanying experimental verification has been lacking, with the exception of the work of Ref. 7. Regarding power factor gains, experimental demonstration, to the best of our knowledge, is completely lacking. The work of Refs. 12 and 16 has demonstrated very high power factors in Si-based nanocomposites, but energy filtering was only partially responsible for this. Surprisingly, despite the fact that the energy-filtering idea was suggested in 1998,⁵ theoretical investigation of why power factor benefits are hard to realize experimentally has still not been carried out.

(Received June 15, 2015; accepted October 5, 2015;
published online November 3, 2015)

In this work, we use the nonequilibrium Green's function (NEGF) method to demonstrate that, although σS^2 can be theoretically improved within an optimized geometry, different types of variation from the idealized shape act as strong detrimental mechanisms. We show that variations in the shape of the potential well, the shape of the potential barrier, and most importantly the width of the barriers can to a large degree destroy the energy-filtering benefits. Thus, this work could partially shed light on the lack of experimental validation of theoretical claims with respect to energy filtering in cross-plane superlattices. The paper is organized as follows: In “[Methods](#)” section we briefly describe the methods used, referring to the literature for more elaborate discussions of the models and numerical formulation. In “[Results and Discussion](#)” section we describe and discuss the results, and finally in “[Conclusions](#)” we conclude.

METHODS

We use the NEGF method in the effective mass approximation, including both acoustic and optical phonon scattering. This method amounts to a nonequilibrium extension of many-body perturbation theory and is a numerical implementation of the Keldysh–Kadanoff–Baym formalism. The main object of the theory is the nonequilibrium Green's function

$$G(E) = [(E - i\eta) - H - \Sigma_1 - \Sigma_2 - \Sigma_{\text{scatt}}]^{-1}, \quad (1)$$

which holds information about the density of states and energy spectrum of the system, and

$$G^{n/p} = G \Sigma^{\text{in/out}} G^+ \quad (2)$$

holds information about the occupancy of states, where

$$\Sigma^{\text{in/out}} = \Sigma_{\text{scatt}}^{\text{in/out}} + \Sigma_1^{\text{in/out}} + \Sigma_2^{\text{in/out}}. \quad (3)$$

In these equations, H is the Hamiltonian of the channel of interest, $i\eta$ is an imaginary infinitesimal, and $\Sigma_{1,2}$ and Σ_{scatt} are the perturbative self-energies capturing the effect of the left and right contacts and the scattering processes (acoustic and optical phonon scattering), respectively. The corresponding $\Sigma_{1,2}^{\text{in/out}}$ is defined as $\Sigma_{1,2}$ times the Fermi–Dirac distribution for “in” or one minus the Fermi–Dirac distribution for “out,” and $\Sigma_{\text{scatt}}^{\text{in/out}}$ is defined below. The scattering self-energies are taken here to have only two components, resulting from optical (Σ_{OP}) and acoustic (Σ_{AP}) phonon scattering. As is common practice, the self-energies of phonon scattering are taken to be diagonal in the real-space basis (amounting to the assumption that phonon scattering is local) and acoustic phonon collisions were assumed to be due to elastic and optical phonons with flat bandstructure. Thus, the self-energies of optical phonons are taken to be

$$\Sigma_{\text{OP}}^{\text{in}}(E) = D_{\text{OP}}(n_\omega + 1)G^n(E + \hbar\omega) + D_{\text{OP}}n_\omega G^n(E - \hbar\omega), \quad (4a)$$

$$\Sigma_{\text{OP}}^{\text{out}}(E) = D_{\text{OP}}(n_\omega + 1)G^p(E - \hbar\omega) + D_{\text{OP}}n_\omega G^p(E + \hbar\omega), \quad (4b)$$

while those of acoustic phonons are taken to be

$$\Sigma_{\text{AP}}^{\text{in/out}} = D_{\text{AP}}G^{n/p}(E). \quad (5)$$

In this formalism, we assume deformation potential scattering, where the strength of electron–phonon scattering by phonons in the self-energies $\Sigma^{\text{in/out}}$ is captured by the constants D_{AP} and D_0 that describe acoustic and optical phonons, as is common practice in electronic transport calculations. We do not compute the phonon spectrum, despite the fact that in a superlattice geometry it could be different compared with bulk. We still use this common approximation as the focus of this work is on electronic transport rather than details of the phonons or heat transport.

An effective mass model was used with a value of $m_{\text{eff}} = 1.0m_e$ (m_e being the mass of a free electron) and lattice spacing of $a_0 = 0.5$ nm. The energy of the optical phonons ($\hbar\omega$) was chosen to be 60 meV, and the values of the acoustic and optical phonon coupling strengths were taken to be equal (i.e., $D_{\text{AP}} = D_{\text{OP}} = D_0$); this was done to minimize the number of tunable parameters in the system. The value of D_0 was chosen as discussed below. For further information on the NEGF method, the reader is referred to the book of Datta,¹⁹ which is entirely dedicated to a pedagogical introduction to the method.

The power factor, GS^2 (where G is the conductance, not the previously introduced Green's function), is calculated from the expression

$$I = GAV + SGAT. \quad (6)$$

For each value of the power factor, the calculation is done twice, initially with a small potential difference and no temperature difference ($\Delta T = 0$) to yield the conductance [$G = I_{(\Delta T=0)}/\Delta V$], then again with a small temperature difference and no potential difference ($\Delta V = 0$) to yield the Seebeck coefficient [$S = I_{(\Delta V=0)}/G\Delta T$]. This method was validated in Ref. 10. Convergence of self-consistent scattering was measured through the requirement of current conservation throughout the system. A convergence value of 5% conservation was chosen (i.e., convergence is reached if the current varies by no more than 5% along the length of the channel). The sharp features of the system required a very large number (~ 1000 s) of convergence steps. One hundred different device structures were simulated overall in order to gather enough data for the effect of non-idealities on the power factor of superlattices. Only the imaginary part of the scattering self-energy was included. The relevant matrix problems were solved

using the recursive Green's function (RGF) method.²⁰

Figure 1 illustrates the simulated one-dimensional (1D) channel geometry. Figure 1a shows the channel as a series of potential barriers, which is the base geometry we consider, while Fig. 1b shows the local density of states (LDOS) (E, x) extracted from the NEGF. Figure 1c shows the charge density in the channel. Note the charge fluctuations in space and energy, formed by quantum interference. Figure 1d shows the current spectrum and how it fluctuates in energy during emission/absorption of optical phonons. The red line above the barriers indicates the average current spectrum energy. This first check indicates that the simulator functions properly as required.

The next step is to calibrate the base geometry to initially provide optimal power factor values from which a study of detrimental effects can be undertaken. Previous works have indicated that, under optimal conditions, the power factor can be improved by up to $\sim 40\%$, compared with pristine material with a flat potential.^{5,10,11,15} For this to be achieved, however, the transport in the wells needs to be semiballistic, where carriers only lose part of their energy before they reach the next barrier.^{6,11} In addition, it was also indicated that ideally the barrier height needs to extend $\sim k_B T$ above the Fermi level.⁶ Finally, the Fermi level needs to be placed high enough in energy to provide carriers with high velocities and conductivity. Thus, in this work we calibrate the geometry, electron–phonon scattering, Fermi level, and barrier height for these optimal conditions and use the calibrated geometry as a base, before we start to consider the influence of nonidealities in the design parameters. The calibration procedure is as follows: (i) A channel of length $L_{\text{ch}} = 20$ nm is considered with flat potential across it. (ii) The position of the Fermi level E_F for maximum ballistic conductance G is identified. The

conductance G versus E_F is shown in Fig. 2a. The position of E_F for maximum G is indicated by the blue dashed line. This is observed at $E_F = 0.14$ eV. (iii) Using that channel and Fermi level, the electron–phonon scattering interaction is increased (i.e., deviating from the ballistic case towards diffusive transport) until the conductance drops to 50% of the ballistic limit (achieving 50% ballisticity in the channel). The value of the electron–phonon interaction used for this is $D_0 = 0.0016$ eV² (see Ref. 21 for details of the formalism and how D_0 is used). Figure 2b shows how the conductance changes in the 20-nm channel versus D_0 , and the 50% ballisticity value is indicated by the red dashed line.

RESULTS AND DISCUSSION

Once the calibration was completed, we proceeded by forming the superlattice geometry and then investigated the performance of energy-filtering processes under unintended variations in the design parameters away from the optimal case, which could be the usual case in experiments. To form the structure geometry, we placed a series of wells and barriers as in Fig. 1a, with the length of the wells being 20 nm and the width of the barriers being 4 nm, with the Fermi level E_F placed at $E_F = 0.14$ eV.

The first parameter we examine is the shape of the barriers/wells. In practice, an ideal rectangular barrier might not be achievable, thus we examine the influence of deviations from the rectangular shape on the performance. In this case, we model the barrier shape as a Gaussian function (see inset of Fig. 3) and vary the variance. For small variances, the barriers will approach a delta function potential, whereas large variances will tend to recover very thick barriers with a limiting case of a single barrier structure. Crucially, we denote this limiting single barrier structure as a “bulk thermoelectric structure” and take it as a comparison case. Should power factor performance be worse than this case, then the superlattice structure offers no enhancement. Thus, power factor values below this point, marked by a dotted magenta line in the figures to follow, represent a loss of all power factor gains from the superlattice structure. Figure 3 shows the power factor versus the Gaussian distribution variance (the shapes of the distributions are also shown in the inset). Structures with different barrier heights from $V_B = 0.14$ eV to 0.18 eV are indicated. Although the barrier height does not have significant qualitative influence on the power factor, the variance can have a strong influence. In the left side of Fig. 3, for delta-shaped potentials, the power factor is significantly lower as a result of increasing quantum-mechanical tunneling from the barriers, which significantly degrades the Seebeck coefficient. However, at the right side of Fig. 3, the power factor approaches that of the pristine, flat-potential material (magenta dashed line) as expected, since

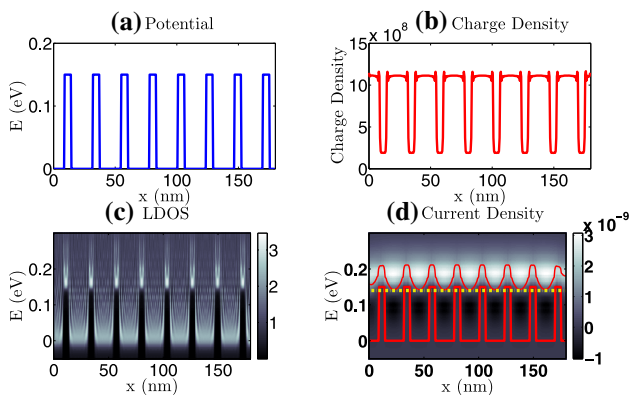


Fig. 1. Sample data for a nanocomposite channel. (a) The potential profile of the barriers in the channel with width of 4 nm and height of 0.16 eV. (b) The local density of states in the channel. (c) The charge density. (d) The current density versus position (colormap). Superimposed on the image are the potential barriers and the carrier energy expectation value $\langle E \rangle$.

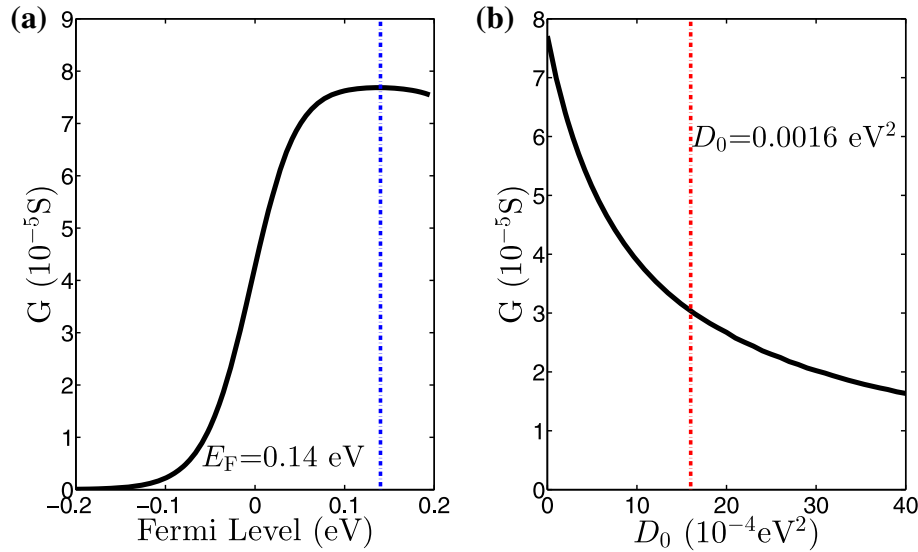


Fig. 2. Calibration of the model and initial channel material. A channel of length $L_{\text{ch}} = 20$ nm is used. (a) The position of the Fermi level for maximum ballistic conductance G is identified. The maximum conductance is observed for $E_F = 0.14$ eV. (b) Using that channel and Fermi level, the electron–phonon interaction is increased until the conductance drops to 50% of the ballistic limit (achieving 50% ballisticity).

the barriers become significantly thicker with the variance. In the middle region, however, an improvement of the power factor is observed for variances around 0.7 nm^2 , resulting in a power factor value similar to the optimal one achieved with square barriers (see Fig. 5). Thus, these results indicate that the shape of the barriers is important, and care needs to be taken in their design, especially to avoid the possibility of tunneling.

To further stress the detrimental effect of quantum-mechanical tunneling from thin barriers, the left axis of Fig. 4 (black) shows the power factor versus barrier width for the starting geometry with perfect, square-shaped barriers. Indeed, similarly to Fig. 3, in the left side, thin barriers allow significant tunneling, which degrades the Seebeck coefficient and diminishes the power factor. As the width increases, the power factor increases, but then for larger widths the power factor begins to drop slightly again, and in the limit of infinite barrier width it approaches the single barrier, flat-potential channel. The reason is that the channel resistance increases with the barrier width as carriers relax near the bottom of the barrier conduction band more effectively. Carrier velocities and conductivity at those energy regions are low. The less the barrier space in the channel, the better the conductivity, but a large amount of tunneling should be avoided. An optimal point can be found in the middle region for barrier width of $W = 3$ nm, which is thick enough to prevent sufficient tunneling to erode the energy-filtering effect but thin enough to prevent resistance increase. To further demonstrate that the power factor loss for ultrathin barriers is due to an increase in tunneling and that the amount of tunneling for barriers above $W = 3$ nm is not sufficient to further erode the power factor, the right axis of

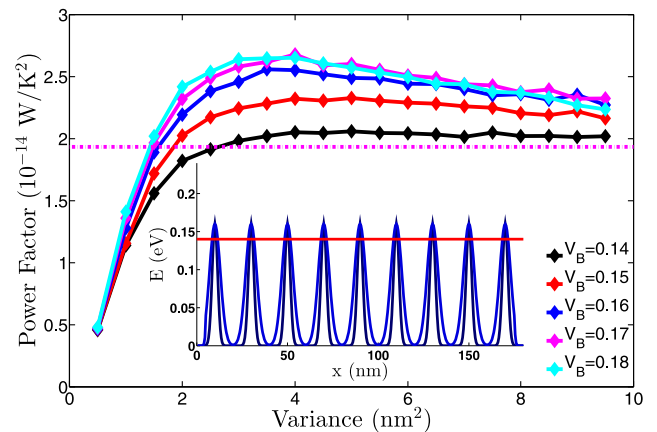


Fig. 3. Power factor of a superlattice material geometry upon deviations of the shape of the barriers/wells from a square to a Gaussian-like shape. Materials with different barrier heights from $V_B = 0.14$ eV to 0.18 eV are shown. Inset: The potential profiles in channels with Gaussian-shaped barriers and wells.

Fig. 4 (blue) shows the ratio of the current contribution from tunneling to the total current. Indeed, tunneling decreases monotonically, contributing only $\sim 35\%$ at $W = 3$ nm. This can be quite significant, but its effect on the power factor is limited. It is also clear that the sudden drop in power factor for $W < 2$ nm, going even below the magenta line, coincides with the increase in the fraction of the total current tunneling through the barriers.

The final nonideality we examine is the effect of well shape alone. The motivation for this is to isolate the effect of the barrier shape and the well shape, in order to better understand the nonidealities in the shape of the well. For this, we consider a flat-top rectangular barrier with fixed thickness, but allow for a decay of the potential into the well

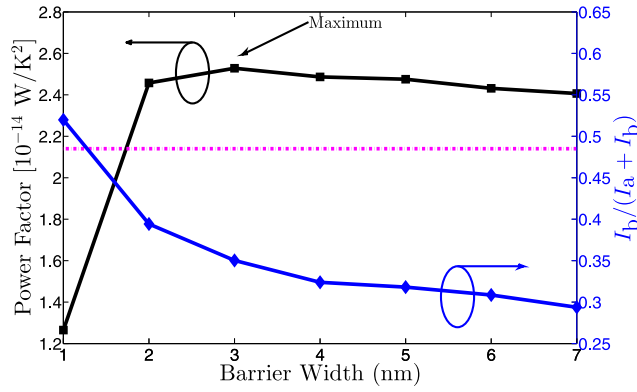


Fig. 4. Left axis (black): Power factor versus barrier width. The optimal barrier width is ~ 3 nm, which is thick enough to prevent a large amount of tunneling but thin enough to keep the electrical resistance from barriers low. For very thin barriers (< 3 nm) the power factor drops rapidly, becoming worse than the bulk thermoelectric case (magenta line). Right axis (blue): The fraction of the current that is contributed by tunneling I_b (i.e., flows below the barriers) compared with the total current, flowing above and below the barriers, $I_a + I_b$. It is clear that the dramatic loss in power factor for ultrathin barrier widths coincides with the increase in tunneling current through the barriers.

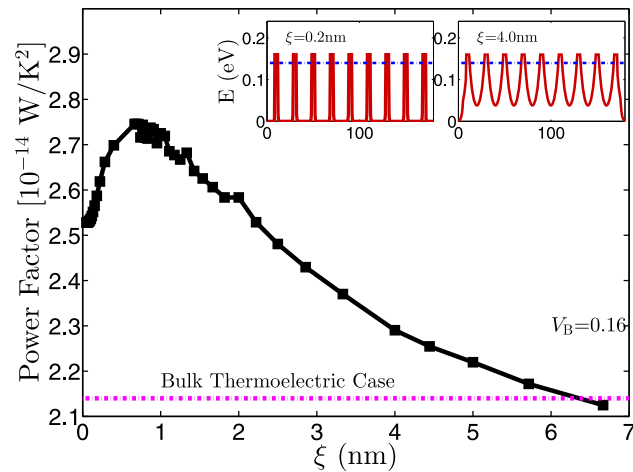


Fig. 5. Power factor versus barrier shape, defined as an exponentially decaying profile described by a decay length ξ from the top of the barrier. The limit $\xi = 0$ corresponds to a square barrier (left side), which is found to be the optimal one. Insets: Potential profiles in the superlattice structure under different values of ξ .

with a decay length ξ as shown in the insets of Fig. 5a and b. The rectangular barriers are ideal (left-side limit of $\xi = 0$), which shows that $\sim 30\%$ improvement can be achieved compared with the bulk TE material case with a flat potential (magenta dashed line). As we deviate from that shape, the power factor drops (approaching the bulk case, right side). For this to happen, however, significant distortion needs to be applied to the shape of the well (compare right versus left inset in Fig. 5).

CONCLUSIONS

Using the NEGF method, we computed the thermoelectric power factor in nanocomposite channels

in the presence of energy barriers designed to enhance filtering and thereby the thermoelectric power factor. While ideally, as shown in previous works,^{5,10,11,15} power factor improvements of up to 30% can be achieved using energy filtering under optimal conditions, we show that this improvement is sensitive to structural imperfections. Fluctuations in the barrier width, barrier shape, and well shape could degrade the performance significantly and take away most of the power factor improvements provided by the superlattice geometry. Especially, barriers with width or shape that allows significant quantum-mechanical tunneling cause large degradation of the power factor. Our results indicate that superlattice thermoelectric material designs should be fabricated close to ideal geometries if benefits are to be provided, which might be an indication as to why significant power factor benefits due to energy filtering have not been observed to date.

ACKNOWLEDGEMENTS

We acknowledge the Vienna Scientific Computing Cluster for computational resources, and funding from the Austrian Science Fund FWF (Project Code P25368-N30).

REFERENCES

1. M. Zebarjadi, K. Esfarjani, M.S. Dresselhaus, Z.F. Ren, and G. Chen, *Energy Environ. Sci.* 5, 5147 (2012).
2. L.D. Zhao, S.H. Lo, J.Q. He, L. Hao, K. Biswas, J. Androulakis, C.I. Wu, T.P. Hogan, D.Y. Chung, V.P. Dravid, and M.G. Kanatzidis, *J. Am. Chem. Soc.* 133, 20476 (2011).
3. D.M. Rowe and G. Min, *AIP Conf. Proc.* 316, 339 (1994).
4. Y. Nishio and T. Hirano, *Jpn. J. Appl. Phys.* 36, 170 (1997).
5. G.D. Mahan and L.M. Woods, *Phys. Rev. Lett.* 80, 4016 (1998).
6. D. Vashaee and A. Shakouri, *Phys. Rev. Lett.* 92, 106103 (2004).
7. J.M.O. Zide, D. Vashaee, Z.X. Bian, G. Zeng, J.E. Bowers, A. Shakouri, and A.C. Gossard, *Phys. Rev. B* 74, 205335 (2006).
8. A. Popescu, L.M. Woods, J. Martin, and G.S. Nolas, *Phys. Rev. B* 79, 205302 (2009).
9. A. Shakouri, *Annu. Rev. Mater. Res.* 41, 399 (2011).
10. R. Kim and M. Lundstrom, *J. Appl. Phys.* 110, 034511 (2011).
11. R. Kim and M.S. Lundstrom, *J. Appl. Phys.* 111, 024508 (2012).
12. D. Narducci, E. Selezneva, G. Cerofolini, S. Frabboni, and G. Ottaviani, *J. Solid State Chem.* 193, 19 (2012).
13. W. Liu, X. Yan, G. Chen, and Z. Ren, *Nano Energy* 1, 42 (2012).
14. H. Alam and S. Ramakrishna, *Nano Energy* 2, 190 (2013).
15. N. Neophytou and H. Kosina, *J. Appl. Phys.* 114, 044315 (2013).
16. N. Neophytou, X. Zianni, H. Kosina, S. Frabboni, B. Lorenzi, and D. Narducci, *Nanotechnology* 24, 205402 (2013).
17. J.-H. Bahk, Z. Bian, and A. Shakouri, *Phys. Rev. B* 89, 075204 (2014).
18. J.-H. Bahk and A. Shakouri, *Appl. Phys. Lett.* 105, 052106 (2014).
19. S. Datta, *Quantum Transport: Atom to Transistor* (Cambridge, NY: Cambridge University Press, 2005).
20. R. Lake, G. Klimeck, R.C. Bowen, and D. Jovanovic, *J. Appl. Phys.* 81, 7845 (1997).
21. S.O. Koswatta, S. Hasan, M.S. Lundstrom, and M.P. Anantram, *IEEE Trans. Electron Dev.* 54, 2339 (2007).